CrossMark

ORIGINAL

A study on the optimization of the angle of curvature for a Ranque–Hilsch vortex tube, using both experimental and full Reynolds stress turbulence numerical modelling

Seyed Ehsan Rafiee[1] · Sabah Ayenehpour[2] · M. M. Sadeghiazad[1]

Abstract The working tube is a main part of vortex tube which the compressed fluid is injected into this part tangentially. An appropriate design of working tube geometry leads to better efficiency and performance of vortex tube. In the experimental investigation, the parameters are focused on the working tube angle, inlet pressure and number of nozzles. The effect of the working tube angle is investigated in the range of $\theta = 0$–$120°$. The experimental tests show that we have an optimum model between $\theta = 0$ and $\theta = 20°$. The most objective of this investigation is the demonstration of the successful use of CFD in order to develop a design tool that can be utilized with confidence over a range of operating conditions and geometries, thereby providing a powerful tool that can be used to optimize vortex tube design as well as assess its utility in the field of new applications and industries. A computational fluid dynamics model was employed to predict the performances of the air flow inside the vortex tube. The numerical investigation was done by full 3D steady state CFD-simulation using FLUENT6.3.26. This model utilizes the Reynolds stress model to solve the flow equations. Experiments were also conducted to validate results obtained for the numerical simulation. First purpose of numerical study in this case was validation with experimental data to confirm these results and the second was the optimization of experimental model to achieve the highest efficiency.

List of symbols

D	Diameter of vortex tube (mm)
k	Turbulence kinetic energy ($m^2\,s^{-2}$)
L	Length of vortex tube (mm)
r	Radial distance from the centerline (mm)
T	Temperature (K)
T_i	Inlet gas temperature (K)
Z	Axial length from nozzle cross section (mm)
L	Length (m)
dc	Diameter of cold orifice (m)
$\dot{m}$	Mass flow rate ($kg\,s^{-1}$)
R^*	The radius of vortex-chamber
S	The width of a nozzle
r^*	Truncated cone radius (m)
G	Truncated ratio

Greek symbols

ΔT	Temperature difference (K)
α	Cold mass fraction
Θ	Cone angle
ε	Turbulence dissipation rate ($m^2\,s^{-3}$)
ρ	Density ($kg\,m^{-3}$)
σ	Stress ($N\,m^{-2}$)
μ	Dynamic viscosity ($kg\,m^{-1}\,s^{-1}$)
μ_t	Turbulent viscosity ($kg\,m^{-1}\,s^{-1}$)
τ	Shear stress ($N\,m^{-2}$)
τ_{ij}	Stress tensor components
R_{WT}	The radius of working tube
R_C	The radius of cold orifice
V	Velocity of flow

✉ Seyed Ehsan Rafiee
s.e.rafiee@mee.uut.ac.ir

1   Department of Mechanical Engineering, Urmia University of Technology, Urmia, Iran

2   Department of Mechanical Engineering, Razi University of Kermanshah, Kermanshah, Iran

Subscripts

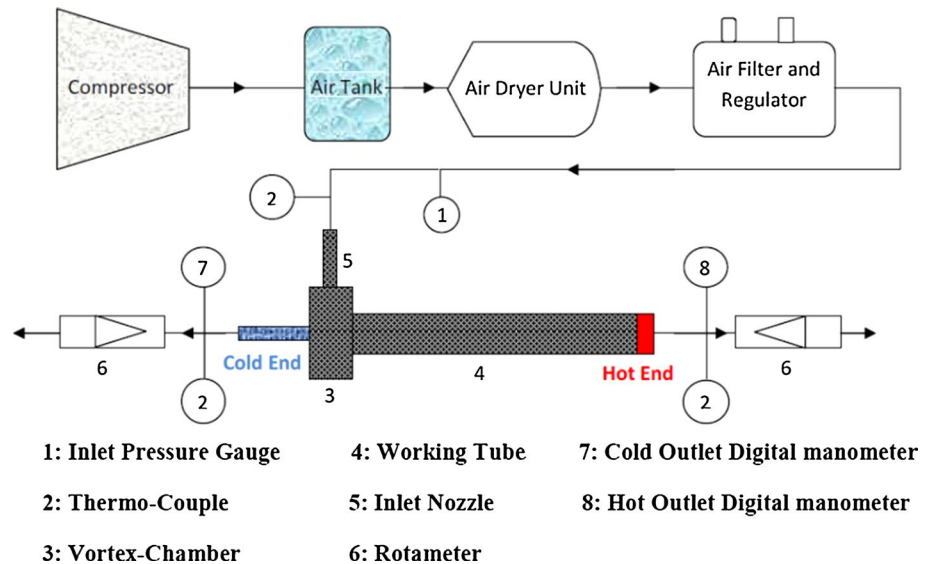|	
in	Inlet
c	Cold
h	Hot
t	Total

1 Introduction

The Ranque–Hilsch vortex tube (RHVT) is a simple device with no moving parts that separates a compressed inlet stream into two cold and hot outlet fluids. This apparatus has many uses such as gas purifying, spot cooling, refrigeration processes and positional solder. Vortex tube was accidentally invented by Ranque [1, 2] (a French physicist) who was studying on the dust separation by vortex tube, and developed by Hilsch [3] (a German physicist) who issued his work through an article in 1947. The hot and cold temperature differences that are denoted by $\Delta T h$ and $\Delta T c$ respectively are the main quantities in this system and are commonly called "temperature separation" criterion. A schematic drawing of a typical vortex tube and its proceeds is shown in Fig. 1. A vortex tube includes different parts such as: one or more inlet nozzles, a vortex-chamber, a cold end orifice, a throttle valve that is located at the end of main tube and a working tube. When pressured fluid is entered into the vortex-chamber tangentially via the nozzles, a strong rotational flow field is created.

When the fluid tangentially swirls to the center of the vortex tube it is expanded and cooled. After occurrence of the energy separation in the vortex tube the pressured inlet fluid stream was divided into two different fluid streams including hot and cold exhaust fluids. The "cold exit or cold orifice" is located at near the inlet nozzles and at the other side of the working tube there is a changeable stream restriction part namely the control or throttle valve which determines the mass flow rate of hot exit. As seen in Fig. 1, a percent of the compressed gas escapes through the valve at the end of the working tube as hot stream and the remaining gas returns in an inner swirl flow and leaves through the cold exit orifice. Opening the throttle valve reduces the cold airflow and closing the valve increases the cold
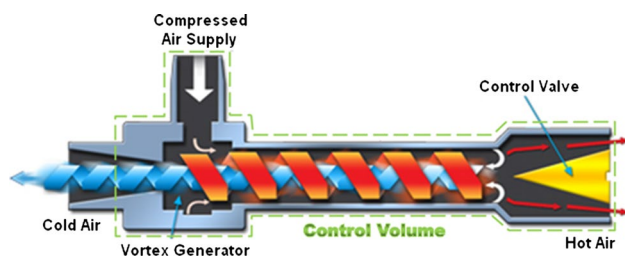
Fig. 1 A schematic drawing of Ranque–Hilsch vortex tube

mass flow ratio. Some of investigations on various aspects of vortex tubes are briefly mentioned below. Valipour and Niazi [4] studied the effect of curved working tube on vortex tube performance. They found that the curvature in the main tube has different effects on the vortex tube performance depending on inlet pressure and cold mass fraction. Also their work presents that the maximum cold temperature difference is created by straight one. Dincer [5] performed an experimental study on vortex tube systems. In his study, performances of vortex tubes were experimentally investigated under three different situations on basis of inlet pressure and the cold mass fraction. 1st situation is the conventional vortex tube. 2nd situation is the threefold cascade type vortex tube (with three RHVTs). 3rd situation deals with the six cascade type RHVT (with six RHVTs). He found that, the best efficiency occurs at the 3rd situation. Xue et al. [6] experimentally tested the effects of the geometrical parameters, such as: inlet nozzles, cold exit, hot exit and the working tube length, were investigated, which presented the settings for the best vortex tube performance. Im and Yu [7] employed a counter-flow type of vortex tube to investigate the energy separation characteristics with various geometric configurations including; nozzle area ratio and pressure inlet and cold exit diameter. This study shows that, variation of the cold exit orifice diameter significantly influences the energy separation between hot exit and cold exhaust. Mohammadi and Farhadi [8] carried out an experimental study to optimize the vortex tube parameters. In their study, a simple vortex tube with various parts is employed to obtain the optimum nozzle intake numbers and diameter. The influence of inlet pressure and cold mass fraction are also studied. Results illustrate that increasing the nozzle numbers causes a temperature drop and the optimum nozzle diameter corresponds to quarter of working tube diameter. Rafiee and Rahimi [9] performed an experimental work on convergence ratio of nozzles and in their work a three dimensional computational fluid dynamic model was introduced as a predictive tools to obtain the maximum cold temperature difference. Also they proved that energy separation procedure inside the vortex tube can be improved by using convergent nozzle. Saidi and Yazdi [10] presented a new approach to optimize characteristics and operating conditions of a vortex-tube using exergy analysis. Secchiaroli et al. [11] carried out a numerical analysis to investigate the vortex tube performance. Their work is about numerical analysis of the internal flow inside a commercial RHVT operating in jet impingement. Shamsoddini and Nezhad [12] performed a numerical investigation to study the effect of nozzles number on the flow field and efficiency of a vortex tube. In their work the effects of the number of nozzles on the cooling power of a vortex tube are analyzed, using a three-dimensional numerical fluid dynamics model and it is observable

Fig. 2 Schematic diagram of the experimental setup

1: Inlet Pressure Gauge **4: Working Tube** **7: Cold Outlet Digital manometer**

2: Thermo-Couple **5: Inlet Nozzle** **8: Hot Outlet Digital manometer**

3: Vortex-Chamber **6: Rotameter**

that as the nozzle number is increased, cooling power increases significantly while the temperature of cold outlet decreases. Murat et al. [13] introduced an optimization of performance of vortex tube using Taguchi method. Their study shows the application of Taguchi method in assessing maximum temperature difference for the vortex tube performance. Chang et al. [14] experimentally investigated the effect of divergent hot tube on vortex tube performance. In their work, the parameters are focused on some geometrical characteristics including divergence angle of divergent hot tube, length of divergent hot tube and number of nozzles. Experimental results show that there is an optimal angle to achieve the highest refrigeration efficiency, and 4° is the optimal candidate under their experimental tests. Stephan et al. [15] maintained that Gortler vortices form on the inside wall of the working tube and drive the fluid motion. Dincer et al. [16] experimentally investigated the distinction between the hot and cold streams of vortex tubes with different length to diameter ratios (L/D). Akhesmeh et al. [17] made a sectional 3D CFD model to study the variation of velocity, pressure and temperature inside a vortex tube. Their results obtained upon the numerical approach comprehensively emphasized on the mechanism of hot peripheral flow and a reversing inner cold core flow formation.

2 Experimental study

In this investigation, a counter flow RHVT with (L = 250 mm, D = 18 mm) L/D ratio equal to 13.88 was applied. Seven different working tubes with different bending angles (θ = 5, 10, 20, 40, 70, 90 and 120) have been manufactured and used in the tests as shown in Fig. 3. The schematic diagram of the test setup is shown in Fig. 2. The

inlet pressures of the counter flow vortex tube have been measured by use of a pressure gauge (±0.5 %) as shown in Fig. 2. The mass flow rates at the cold and hot exhausts of the counter flow vortex tube have been determined by use of rotameters. The temperatures of the pressurized air at the inlet, and the cold and hot exits were determined by employing of a digital thermometer with ±0.2 °C precision tolerances, and the measured temperature magnitudes have been changed into Kelvin (K) unit. The throttle valve has been placed on the hot outlet of the main tube in order to adjust the mass flow rate of the hot air. Before starting the experimental tests, the control valve on the hot outlet was set in fully open situation. And then the air tank was worked and by use of the valve that was applied on the vortex tube inlet position, the beginning pressure value of 0.4 MPa was gained. And during this procedure, the mass flow rates and pressures of the air at the cold exhaust and hot exit were determined by using rotameters and pressure gauges, respectively. The experimental tests were performed several times for the entire working tubes used in this investigation.

The schematic diagram of the experimental setup is shown in Fig. 2.

3 Governing equations

The compressible turbulent and highly rotating fluid stream is considered inside the designed vortex tube to be three-dimensional (3D), steady state, and employs Reynolds stress equations (RSM) theory on the basis of the finite volume method. Consequently, the governing equations are assumed and arranged by the conservation of mass, momentum, and energy equations.

The equation for continuity equation can be presented as bellow:

$$\frac{\partial \rho}{\partial t} + \nabla.(\rho \vec{v}) = S_m \tag{1}$$

The fluid flow in this work has been considered 'steady' and term S_m is the mass added to continuous domain from other domains.

Momentum equation

$$\frac{\partial}{\partial x_j}(\rho\, u_i u_j) = -\frac{\partial p}{\partial x_i} + \frac{\partial}{\partial x_j}\left[\mu\left(\frac{\partial u_i}{\partial x_j} + \frac{\partial u_j}{\partial x_i} - \frac{2}{3}\delta_{ij}\frac{\partial u_k}{\partial x_k}\right)\right]$$
$$+ \frac{\partial}{\partial x_j}(-\bar{\rho}\bar{u}'_i\bar{u}'_j) \tag{2}$$

Energy equation

$$\frac{\partial}{\partial x_i}\left[u_i\,\rho\left(h + \frac{1}{2}u_j u_j\right)\right] = \frac{\partial}{\partial x_j}\left[k_{eff}\frac{\partial T}{\partial x_j} + u_i(\tau_{ij})_{eff}\right], \quad k_{eff}$$
$$= K + \frac{c_p\,\mu_t}{\Pr_t} \tag{3}$$

Since we considered the working gas is an ideal gas, then the compressibility effect should be assumed as follow:

$$p = \rho RT \tag{4}$$

The Reynolds stress model (RSM) [18–20] is the most elaborate turbulence model that this paper provides. Abandoning the isotropic eddy-viscosity hypothesis, the RSM closes the Reynolds-averaged Navier–Stokes equations by solving transport equations for the Reynolds stresses, together with an equation for the dissipation rate. This means that five additional transport equations are required in 2D flows and seven additional transport equations must be solved in 3D. Since the RSM accounts for the effects of streamline curvature, swirl, rotation, and rapid changes in strain rate in a more rigorous manner than one-equation and two-equation models, it has greater potential to give accurate predictions for complex flows. However, the fidelity of RSM predictions is still limited by the closure assumptions employed to model various terms in the exact transport equations for the Reynolds stresses. The modeling of the pressure-strain and dissipation-rate terms is particularly challenging, and often considered to be responsible for compromising the accuracy of RSM predictions. The RSM might not always yield results that are clearly superior to the simpler models in all classes of flows to warrant the additional computational expense. However, use of the RSM is a must when the flow features of interest are the result of anisotropy in the Reynolds stresses. Among the examples are cyclone flows, highly swirling flows in combustors, rotating flow passages, and the stress-induced secondary flows in ducts. The exact form of the Reynolds stress transport equations may be derived by taking moments of the exact momentum equation. This is a process wherein the exact momentum equations are multiplied by a fluctuating property, the product then being Reynolds-averaged. Unfortunately, several of the terms in the exact equation are unknown and modeling assumptions are required in order to close the equations.

The exact transport equations for the transport of the Reynolds stresses, $\rho\overline{u'_i u'_j}$, may be written as follows:

$$\frac{\partial}{\partial t}(\rho\overline{u'_i u'_j}) + \underbrace{\frac{\partial}{\partial x_k}(\rho u_k\overline{u'_i u'_j})}_{C_{ij}}$$
$$= \underbrace{-\frac{\partial}{\partial x_k}[\rho\overline{u'_i u'_j u'_k} + \overline{p(\delta_{kj}u'_i + \delta_{ik}u'_j)}]}_{D_{T,ij}} + \underbrace{\frac{\partial}{\partial x_k}[\mu\frac{\partial}{\partial x_k}\overline{u'_i u'_j}]}_{D_{L,ij}}$$
$$\underbrace{-\rho(\overline{u'_i u'_k}\frac{\partial u_j}{\partial x_k} + \overline{u'_j u'_k}\frac{\partial u_i}{\partial x_k})}_{P_{ij}} - \underbrace{\rho\beta(g_i\overline{u'_j\theta} + g_j\overline{u'_i\theta})}_{G_{ij}}$$
$$+ \underbrace{\overline{p(\frac{\partial u'_i}{\partial x_j} + \frac{\partial u'_j}{\partial x_i})}}_{\phi_{ij}} \underbrace{-2\mu\overline{\frac{\partial u'_i}{\partial x_k}\frac{\partial u'_j}{\partial x_k}}}_{\varepsilon_{ij}}$$
$$\underbrace{-2\rho\Omega_k(\overline{u'_j u'_m}\varepsilon_{ikm} + \overline{u'_i u'_m}\varepsilon_{jkm})}_{F_{ij}} + S_{user} \tag{5}$$

In this equation $\frac{\partial}{\partial t}(\rho\overline{u'_i u'_j})$, C_{ij}, DT, ij, DL, ij, P_{ij}, G_{ij}, ϕ_{ij}, ε_{ij}, F_{ij} and Suser are defined as local time derivative, convection, turbulent diffusion, molecular diffusion, stress production, Buoyancy production, pressure strain, dissipation, Production By System Rotation and User-Defined Source Term respectively. Of the various terms in these exact equations C_{ij}, DL, ij, P_{ij} and F_{ij} do not require any modeling. But DT, ij, G_{ij}, ϕ_{ij} and ε_{ij} need to be modeled to close the equations.

Finite volume method with a 3D structured mesh is applied to the governing equations, which is one of the numerical approaches to describe complex flow patterns in the vortex tube. Inlet air is considered as a compressible working fluid, where its specific heat, thermal conductivity and dynamic viscosity are taken to be constant during the numerical analysis procedure. Second order upwind scheme is utilized to discretize convective terms, and SIMPLE algorithm is used to solve the momentum and energy equations simultaneously. Because of highly non-linear and coupling virtue of the governing equations, lower under-relaxation factors ranging from 0.1 to their default amount are taken for the pressure, density, body forces, momentum, turbulent viscosity and energy components to ensure the stability and convergence of the iterative calculations.

3.1 Physical model description

3.1.1 3D CFD model

The 3D CFD model created in this work is based on that employed by authors in the all of experimental tests. The experimental device used was a vortex tube for cooling purposes. The dimensional geometry of this vortex tube has been presented in Table 1. In numerical simulation and experimental investigation, all geometrical properties of experimental model are kept constant but seven different bending angles were used instead of one. The radius of

Table 1 Geometrical characteristics of vortex tube used for experiment and CFD models

	Length of working tube	Diameter of working tube	Diameter of cold exit	Number of nozzle	Control valve	Main tube
Present Work	250 mm	18 mm	9 mm	2, 3, 4, 6	Truncated cone	Curved, straight
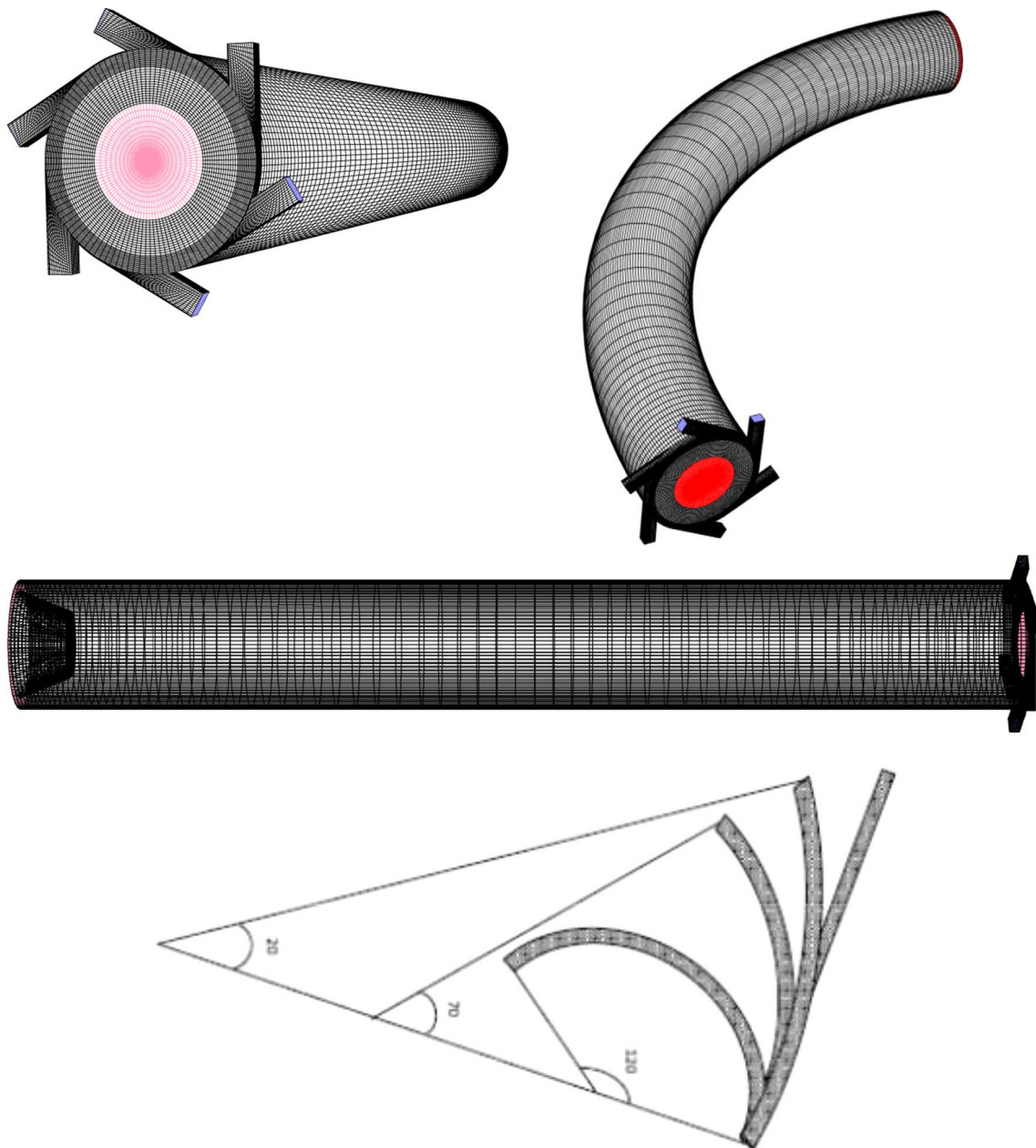
Fig. 3 3D CFD model of vortex tube and working tube shape

the vortex tube was fixed at 9 mm, and the length of main tube is 250 mm. In these models, a regular organized mesh grid has been employed. All radial lines of this model of meshing were joined to the centerline of vortex tube and the circuit lines were regularly designed from wall to the centerline of vortex tube. So, the volume units created are completely regular cubic volumes in this simulation. This meshing system leads to the faster computations, and the procedure of computations was done more precisely.

The schematic forms of 3D CFD model and bending angle are shown in Fig. 3.

Because of highly non-linear and coupling virtue of the governing equations, lower under-relaxation factors ranging from 0.1 to their default amount are taken for the pressure, density, body forces, momentum, turbulent viscosity and energy components to ensure the stability and convergence of the iterative calculations the computations were done by using the FLUENTTM software package. The number of iterations in our computations was located in range of 65,000–70,000. The change of values for under-relaxation factors are shown in Table 2 step by step.

3.1.2 Boundary conditions

Boundary conditions for this study have been indicated in Fig. 4. The inlet is modeled as pressure inlet boundary condition. The inlet stagnation temperature and the pressure inlet are fixed to 294.2 K and 0.4 MPa respectively, according to the experimental conditions.

A no-slip boundary condition is used on all walls of the system. The cold and hot exits boundary condition can be considered as the pressure-far-field (a vortex tube usually works under the ambient conditions and for changes in the cold mass fraction one needs to change the area of hot exit). So the boundary conditions can be summarized as below:

1. At the nozzle inlets, compressed air is modeled as Pressure inlet, with specified pressure value at 4 bar and stagnation temperature fixed at 294.2 K.
2. Cold and hot exit set as pressure-far-field.

3. The wall of the vortex tube is assumed to be insulated and with no slip conditions.

3.2 Grid independence study

We define the "average volume cell" as below:

$$v = \frac{V}{n} \tag{6}$$

where, V is the total volume of the computational domain and n is the number of cells created inside the computational domain. So the average unit cell volume is the ratio of the total volume to the number of cells.

The numerical simulation has been done for several average unit cell volumes in vortex tube system as a computational domain. The grid independency study is for the reason that removing probable errors arising due to grid coarseness. So, first the grid independence study has been done for cold mass fraction $\alpha = 0.24$. As shown in the Fig. 6, at this cold mass ratio the vortex tube reaches a minimum cold exhaust gas temperature. Consequently, in the most of the computations we use $\alpha = 0.24$ as a special cold mass fraction value.

The gradient of cold exit temperature difference as the main parameter is shown in Fig. 5 for different unit cell volumes. Not much major influence can be found in reducing of the unit cell volume size below 0.041 mm^3; which corresponds to 1,325,000 cells.
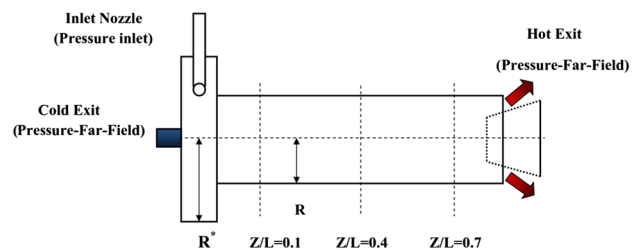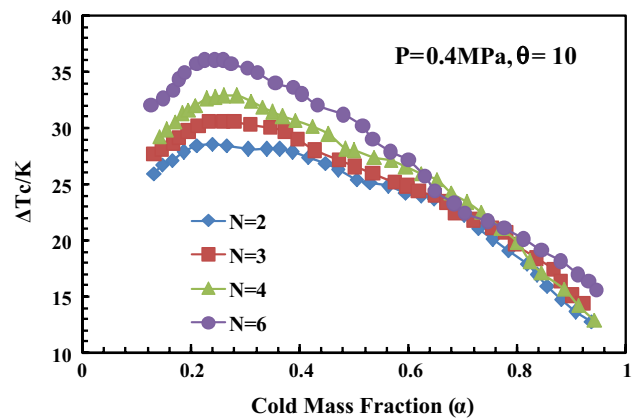

Fig. 4 A schematic form of boundary conditions

Table 2 Under-relaxation factors used for computations

| Under-relaxation factor	Default value	Step 1	Step 2	Step 3	Step 4	Step 5	Step 6
Pressure	0.3	0.1	0.2	0.3	0.3	0.3	0.3
Density	1	0.1	0.4	0.6	0.8	0.9	1
Body force	1	0.1	0.4	0.6	0.8	0.9	1
Momentum	0.7	0.1	0.3	0.5	0.6	0.7	0.7
Turbulent kinetic energy	0.8	0.1	0.3	0.5	0.7	0.8	0.8
Turbulent dissipation rate	0.8	0.1	0.3	0.5	0.7	0.8	0.8
Turbulent viscosity	1	0.1	0.4	0.6	0.8	0.9	1
Reynolds stresses	0.5	0.1	0.2	0.3	0.4	0.5	0.5
Energy	1	0.1	0.4	0.6	0.8	0.9	1
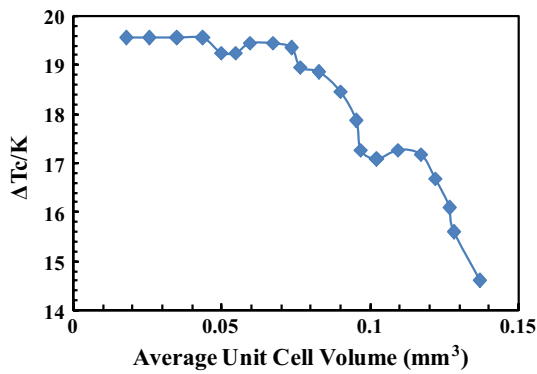
Fig. 5 Grid size independence study on cold temperature difference at different average unit cell volume

Fig. 6 Influence of the bending angle of main tube on the cold temperature difference

Fig. 7 Effect of the number of nozzle on the cold temperature difference
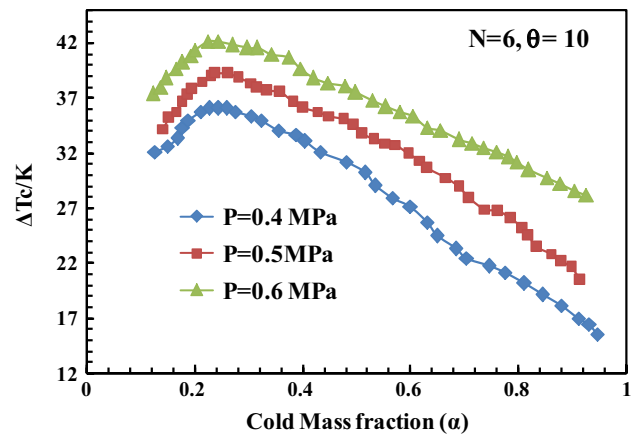
Fig. 8 Cold temperature difference as functions of the cold mass fraction with various pressures

4 Results and discussion

In this study the performance of the vortex tube with L/D = 13.88 and N = 2, 3, 4, 6 was tested under the Pi = 0.4, 0.5 and 0.6 MPa with compressed air. The cooling ΔT_c and the heating ΔT_h effects of the vortex tube are defined as follows, respectively:

$$\Delta T_c = T_i - T_c \tag{7}$$

$$\Delta T_h = T_h - T_i \tag{8}$$

In general, the performance of the vortex tube was defined as the difference between the heating effect and the cooling effect. Subtracting Eq. (7) from (8) gives the vortex tube performance equation as below:

$$\Delta T = T_h - T_c \tag{9}$$

The cold mass fraction or cold mass ratio is one of the important parameters since it indicates the vortex tube performance and the energy separation inside the vortex tube. Cold mass fraction is defined as the percentage of the pressurized air input to that released through the cold end of the tube and can be calculated by using Eq. (10). The cold mass fraction can be controlled by the throttle valve, which is placed at the hot end of the main tube. This can be expressed as follows:

$$\alpha = \frac{\dot{m}_c}{\dot{m}_i} \tag{10}$$

For each of the models used in the simulations and experimental results, the minimum cold exit temperature value was measured when α = 0.24.

The results obtained from the tests (numerical simulation and experimental tests), which involve the effect of bending angle, number of nozzle intakes and the pressure at the inlets on the vortex tube performance, are presented in this section.
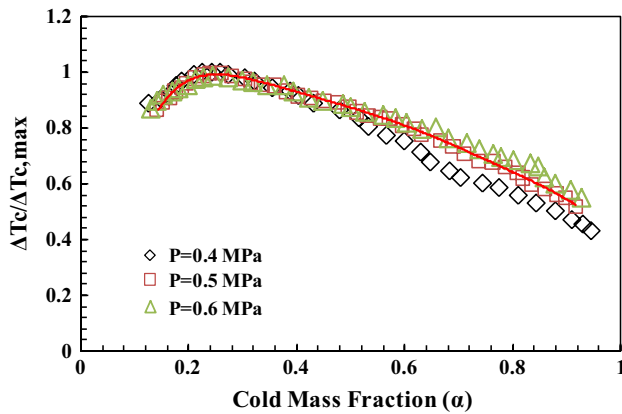
Fig. 9 Non-dimensional cold temperature difference versus cold mass fraction
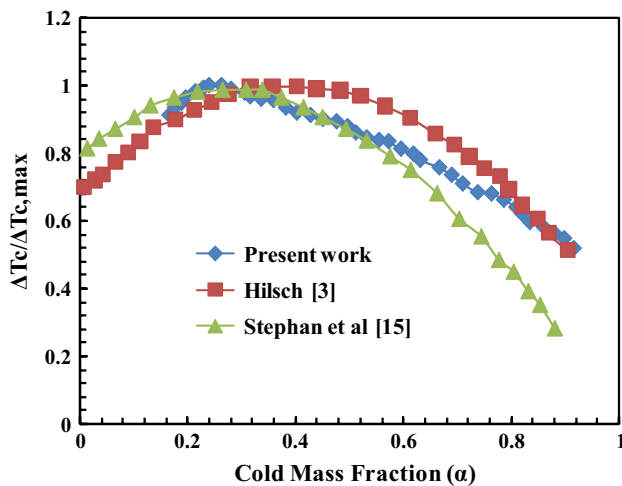
Fig. 10 Comparison of similarity relations obtained by different works

4.1 Experimental results

Typical angles mentioned below have been employed to investigate the performance of the vortex tube refrigerator with the straight nozzle. To expose the effect of bending angles on the temperature reduction (Fig. 6), seven different bending angles i.e. θ = 5, 10, 20, 40, 70, 90 and 120 are tested by using a constant working tube with length of L = 250 mm. The number of nozzle intake is N = 2.

Figure 6 shows the variation in ΔTc for bending angles at different cold mass fractions with inlet pressure of 0.4 MPa. These models were tested and the thermal performance was analyzed while the cold mass fraction was variable. The results indicate that there is optimal value for θ to obtain the highest refrigeration efficiency. According to the results, the cold temperature difference increased when we take into account the effect of bending angle in the range of straight to 10°. Valipour and Niazi [4] studied the effect of curved working tube on vortex tube performance for great bending angles, previously. They found that the great curvature in the main tube (θ = 60 and 110°) has different effects on the vortex tube performance depending on inlet pressure and cold mass fraction. Also their work presents that the maximum cold temperature difference is created by straight compared to curved one. Our results confirm their results for great angles, completely. But in their work, smaller angles have not been tested. We claim that the curved vortex tube can produce the lower cold temperature compared to straight one, but this take placed for smaller bending angles such as θ = 5 and 10°.

On basis of the conclusions for straight nozzles, some reported that increasing the number of nozzles can produce a strong swirling flow field inside the vortex tube and consequently help to improve the temperature separation procedure whereas, some researchers [21] said that the vortex tubes performance decreases with the increase of the nozzles number due to the development of the turbulent flow filed. To indicate the effect of the intake number on the cryogenic capacity of vortex tubes with straight nozzles, N = 2, 3, 4 and 6 nozzles are investigated at inlet pressure of 0.4 MPa with constant parameters θ = 10 and L = 250 mm. Figure 7 indicates the effect of N = 2, 3, 4 and 6 nozzles on the ΔTc of the vortex tube refrigerator with straight nozzles.

Figure 8 shows the effects of inlet pressure on the cold temperature difference at the inlet pressures of 0.4, 0.5 and 0.6 MPa. It is clear that the cold temperature difference is improved by increasing in the inlet pressure. Also the maximum cold temperature difference takes place in the vicinity of α = 0.24 for all inlet pressures of 0.4, 0.5 and 0.6 MPa.

Stephan et al. [15] carried out an approximate investigation for geometrically similar vortex tubes with straight working tube and reported that the ratio of the actual temperature drop of the cold gas that exits from exhaust to the

Table 3 Geometrical characteristics of vortex tubes used by some researchers

	Length of working tube (mm)	Diameter of working tube (mm)	Diameter of cold exit (mm)	Number of nozzle	Shape of main tube
Present work	250	18	9	2, 3, 4, 6	Curved
Hilsch [3]	300	9.2	2.6	1	Straight
Stephan et al. [15]	352	17.6	6.5	1	Straight

Fig. 11 Numerical validation with experimental results for different model of θ
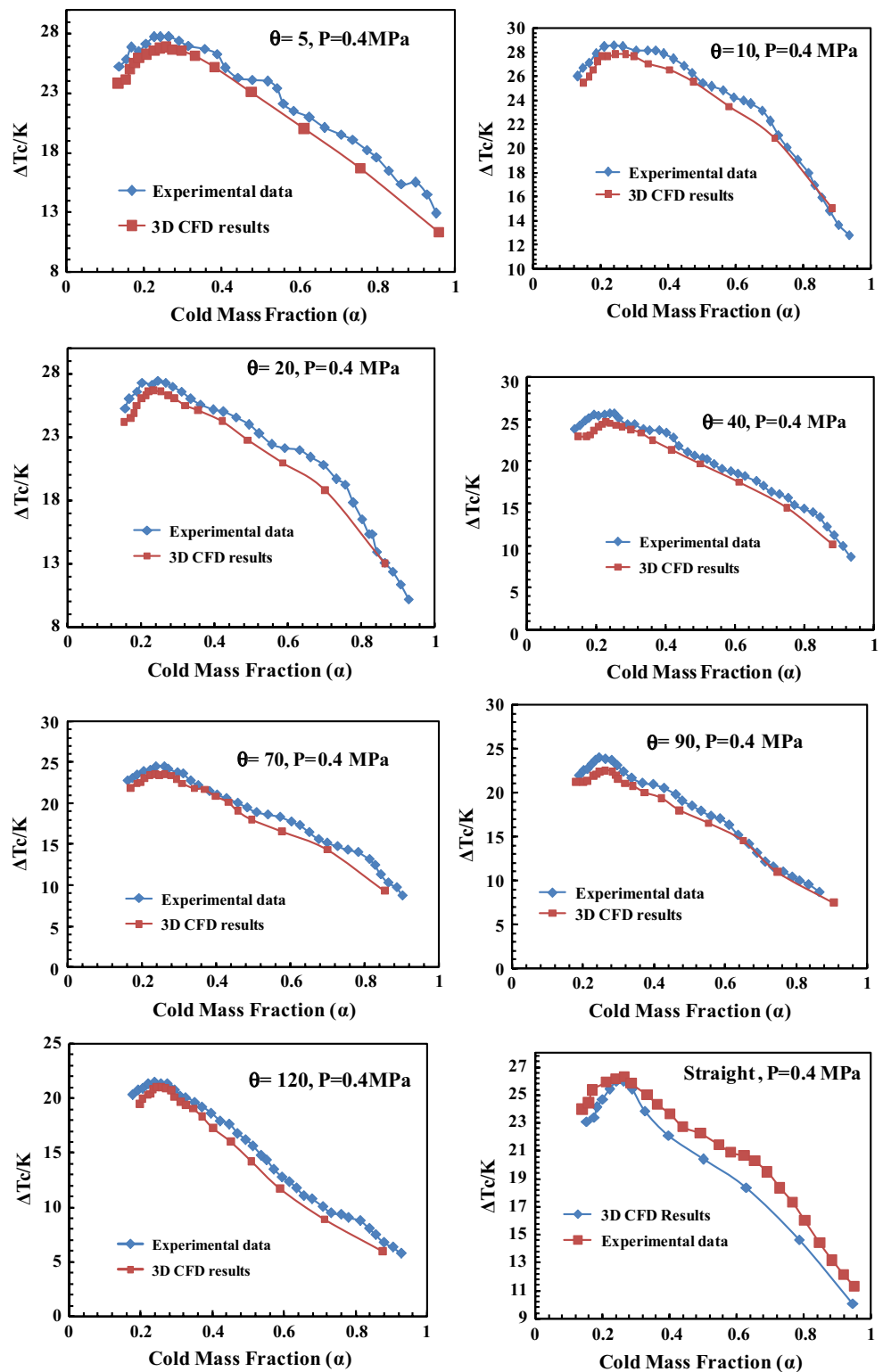
maximum temperature difference $\Delta Tc/(\Delta Tc)max$ can be defined as function of cold mass fraction as below:

$$\frac{\Delta T_c}{\Delta T_{c,\max}} = f(\alpha) \tag{11}$$

In this equation ΔTc is the temperature difference, $(\Delta Tc)max$ is the maximum temperature drop and α is the cold mass fraction and is varied in range from 0 to 1. To investigate the similarity relation for the vortex tube with curved main tube, tests are conducted for a typical vortex

Table 4 The difference between experimental data and simulated results at cold mass fraction 0.24

Model	ΔTc experimental (K)	ΔTc CFD (K)	Difference between experimental and CFD results (%)
Straight Case(f)	26.27	25.98	1.1
$\theta = 5$ Case(d)	26.98	26.84	0.51
$\theta = 10$ Case(x)	28.56	27.79	2.69
$\theta = 20$ Case(r)	27.41	26.63	2.84
$\theta = 40$ Case(v)	25.69	24.74	3.69
$\theta = 70$	24.54	23.59	3.87
$\theta = 90$	23.97	22.54	5.96
$\theta = 120$	21.53	21.07	2.13

tube. The similarity relation $\Delta Tc/(\Delta Tc)max$ as a function of α can be taken and indicated in Fig. 9. It can be introduced as below:

$$\frac{\Delta T_c}{\Delta T_{c,\mathrm{max}}} = -53.88\alpha^6 + 192.2\alpha^5 - 277.6\alpha^4 + 206.8\alpha^3$$
$$- 84.07\alpha^2 + 17.18\alpha - 0.371 \qquad (12)$$

As seen in Fig. 9, the ratio of $\Delta Tc/(\Delta Tc)max$ for vortex tubes with curved main tube is independent of the inlet pressures, and can be presented as a function of the cold mass ratio.

To confirm the similar relation for our vortex tube with curved main tube, results by Stephan et al. [15] and Hilcsh [3] are applied for comparison and the results of this comparison is presented in Fig. 10. This comparison shows that the variation of similar relation in this work is exactly similar to other researches. As seen in Fig. 10, the value of $\Delta Tc/(\Delta Tc)max$ increases with increase in cold mass fraction in the range of 0.19–0.24. With further increase in cold mass fraction the value of mentioned ratio decreases. The geometrical parameters of the vortex tube in their experimental investigations are shown in Table 3.

As seen in Fig. 6, the development trend of ΔTc for seven different bending angles is almost similar. The ΔTc increases with the increase of cold mass fraction up to about $\alpha = 0.24$ and achieves there a maximum value. Thereafter cold temperature difference decreases with the further increase of the cold mass fraction. As seen in Fig. 6, the experimental results present that there is an optimum bending angle to obtain the highest refrigeration efficiency, between 0° and 120° under our experimental conditions, it presents that the vortex tube performance can be ameliorated by using the appropriate bending angle, and there is an optimum value for bending angle of main tube to obtain the highest cryogenic performance.

4.2 Comparisons between CFD results and experimental data

Figure 11 shows the results from the CFD simulation compared to the experimental data. Figure 11 shows that the 3D

CFD has good agreement with the experimental results. All comparisons between the CFD model and the experimental data are reported in terms of the cold mass fraction. The comparison shows that the 3D CFD results can well predict the experimental results. The difference between experimental data and simulated results at cold mass fraction 0.24 are presented in Table 4.

Table 4 indicates that, in this study, CFD data concur well with experimental results. Deviation of the predicted and measured values for the cold temperature difference is less than or equal to 5.96 %.

4.3 Swirl (tangential) velocity and total pressure inside the working tube

In order to demonstrate the effect of change in bending angle on radial profiles of tangential velocity and total pressure, the profiles at two axial locations (Z/L = 0.1 and 0.7) at the cold mass fraction 0.24 were analyzed, the diagrams of which are depicted in Fig. 12.

The diagrams show that at Z/L = 0.1 (near the chamber), the maximum magnitude of tangential velocity in model $\theta = 10$ is 330.844 m/s as the greatest value of all other models, whereas this value is 327.95 m/s for the straight model. This means that the optimization of working tube bending angle leads to an increase in maximum swirl velocity about 1 % near the cold exhaust. In Fig. 12a, b, the radial profiles for the tangential velocity at Z/L = 0.1 and 0.7 are provided for mentioned models. The swirl (tangential) velocity magnitude decreases as we move towards the hot end exit. This is clearly observable that the tangential velocity magnitude in model $\theta = 10$ mm is the greatest swirl velocity among all the created models. Also, the tangential velocity drop magnitude in model $\theta = 5$, 10, and 20 mm is 131.38, 132.37, and 130.75 m/s, respectively, as the greatest swirl velocity drop values among all the models created. This velocity drop is a sign for appropriate energy separation procedure inside the vortex tube. The radial profile of the tangential velocity shows a free vortex near the wall. On the other hand, another forced vortex is
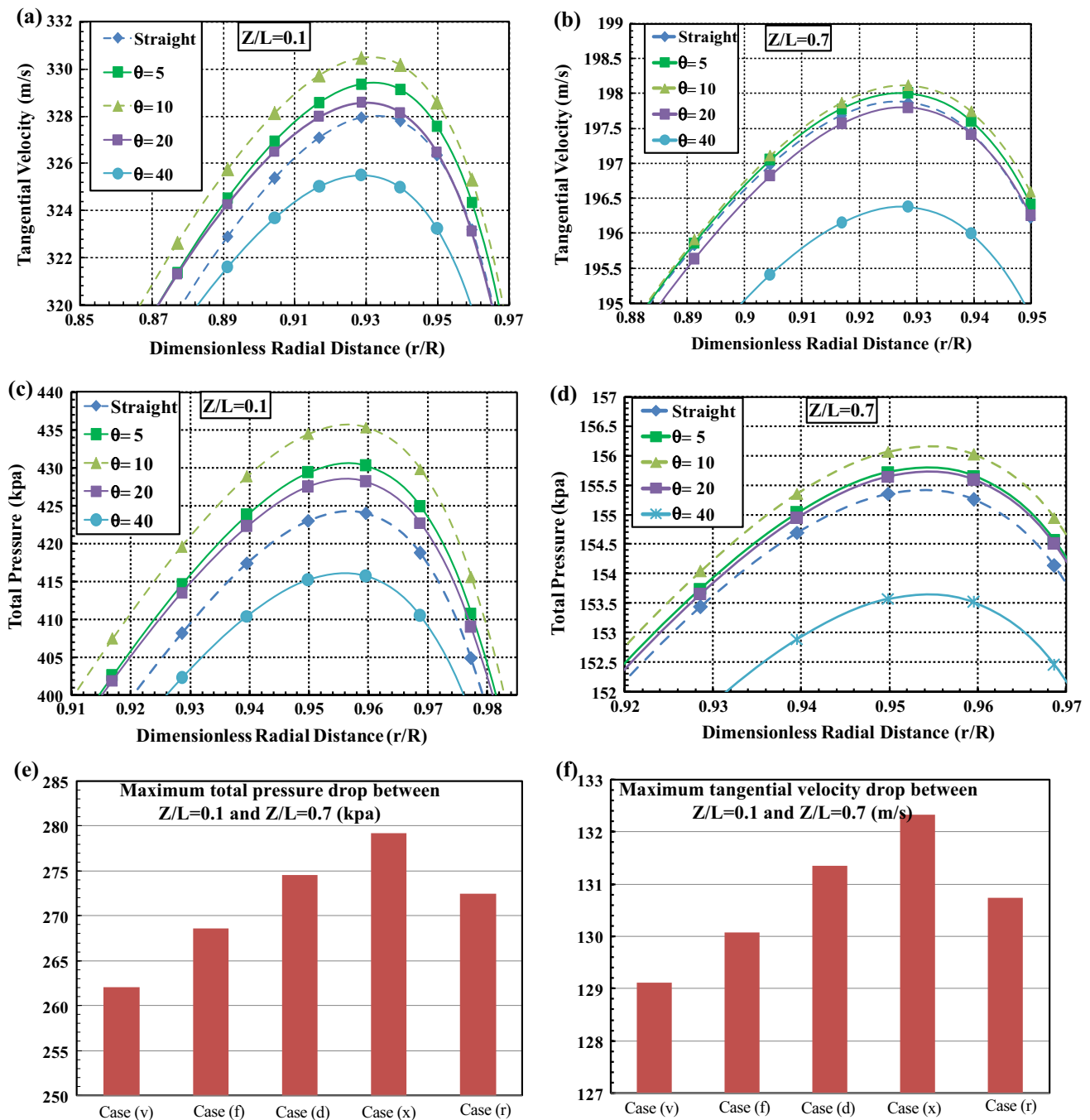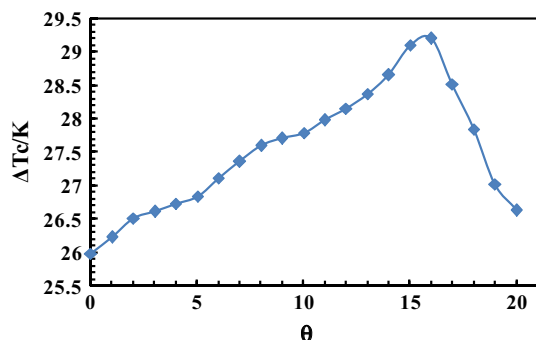
Fig. 12 **a**, **b** Radial profile of tangential velocity at Z/L = 0.1 and Z/L = 0.7 for α = 0.24. **c**, **d** Radial profile of total pressure at Z/L = 0.1 and Z/L = 0.7 for α = 0.24. **e**, **f** Total pressure drop and tangential velocity drop between Z/L = 0.1 and Z/L = 0.7 for the models

formed in the core, in which swirl velocity values decrease as we move towards the centerline of the working tube. The results shown in Fig. 12 are in good coordination with the observations of Gutsol [22]. Figure 12c and d, show the total pressure variations for different bending angle at the two axial locations Z/L = 0.1 and 0.7 as a function

of dimensionless radial distance of the working tube. The maximal magnitude of total pressure is observed near the periphery of the tube wall. As seen in Fig. 12c, d, fluid stream has greater total pressure in θ = 10 in comparison with other cases. Also, the maximum total pressure difference between Z/L = 0.1 and Z/L = 0.7 can be observed

Table 5 The cold temperature difference of all simulated models between θ = 0 and θ = 20

Model	ΔTc
θ = 0	25.98
θ = 1	26.23
θ = 2	26.51
θ = 3	26.61
θ = 4	26.73
θ = 5	26.84
θ = 6	27.11
θ = 7	27.36
θ = 8	27.6
θ = 9	27.71
θ = 10	27.79
θ = 11	27.98
θ = 12	28.15
θ = 13	28.37
θ = 14	28.66
θ = 15	29.11
θ = 16	29.21
θ = 17	28.52
θ = 18	27.85
θ = 19	27.02
θ = 20	26.63

Fig. 13 The graphical plot of the results of Table 5

in Fig. 12e. According to this figure, Case (x) or θ = 10 has the greatest value of pressure drop across the working tube among all the models created. The diagrams show that at Z/L = 0.1, the maximum magnitude of total pressure in model θ = 10 [Case (x)] is 435.8kpa as the greatest value for all the models, whereas this value is 424.2 kpa for the straight model. So, optimization of the bending angle creates an improvement of about 3 % in the maximum total pressure near the cold exit. These results reveal that the temperature reduction of cold air, the total pressure value,

and the tangential velocity value of fluid stream are substantially influenced by the bending angle.

4.4 CFD simulation to find the optimum model

The experiments illustrated that we have an optimum bending angle between θ = 0 and θ = 20. Twenty CFD models have been created with different bending angles between 0 and 20 then the cold temperature difference of these models at α = 0.24 is described in Table 5.

Table 5 indicates that in the range of θ = 0–θ = 20, we have an optimum model which works better than θ = 10° (θ = 10° is the optimal value in first experimental tests, in fact θ = 10° is the optimum value for bending angle before the optimization). This optimal bending angle is θ = 16° (after optimization). According to numerical results the cold temperature difference has increased when we take into account the effect of the bending angle in range of 0–16 and when the bending angle has located in range of 16–20, the cold temperature difference has decreased. The results of this Table can be understood better in Fig. 13. To confirm the results of Table 5, we have selected the optimum model (θ = 16°) and the experiments have done for this model. The cold temperature difference in experimental condition for this model was 29.69 K. According to the experimental results and numerical simulations the optimum model was θ = 16 (after optimization). This is clearly observable that the cold temperature difference magnitude in the model θ = 16 is the greatest cold temperature difference among the all of models. This research indicates that, the value for bending angle of main tubeshould be neither too large nor too small and θ = 16 is the best candidate for achieving the highest ΔTc. The highest ΔTc is 29.69 K for θ = 16 at a cold mass fraction of about 0.24, higher than that of straight around 14 % at the same cold flow fraction. The contours of total temperature of the optimum model for the inlet gas temperature 294.2 K and cold mass fraction 0.24 are shown in Fig. 14 (the contours of optimal curved and straight vortex tubes). As seen in Fig. 14, the vortex tube is an invaluable separator with any moving part which has the ability to separate a high pressure fluid into cold and hot fluid streams. Air separator systems often experience temperature or stream separations in the axial directions (cold and hot streams as Fig. 14). These contours show the temperature distribution inside the vortex tube. According to Fig. 14, the cold stream leaves the main tube at the central region of cold orifice and at other side of vortex tube the hot fluid leaves the main tube through the conical control valve. As a result, the maximum and minimum temperature inside the computational domain is 303 and 263 K respectively. However, the average temperatures at the cold and hot region have been considered.

Fig. 14 Contours of total temperature of the optimum and straight model
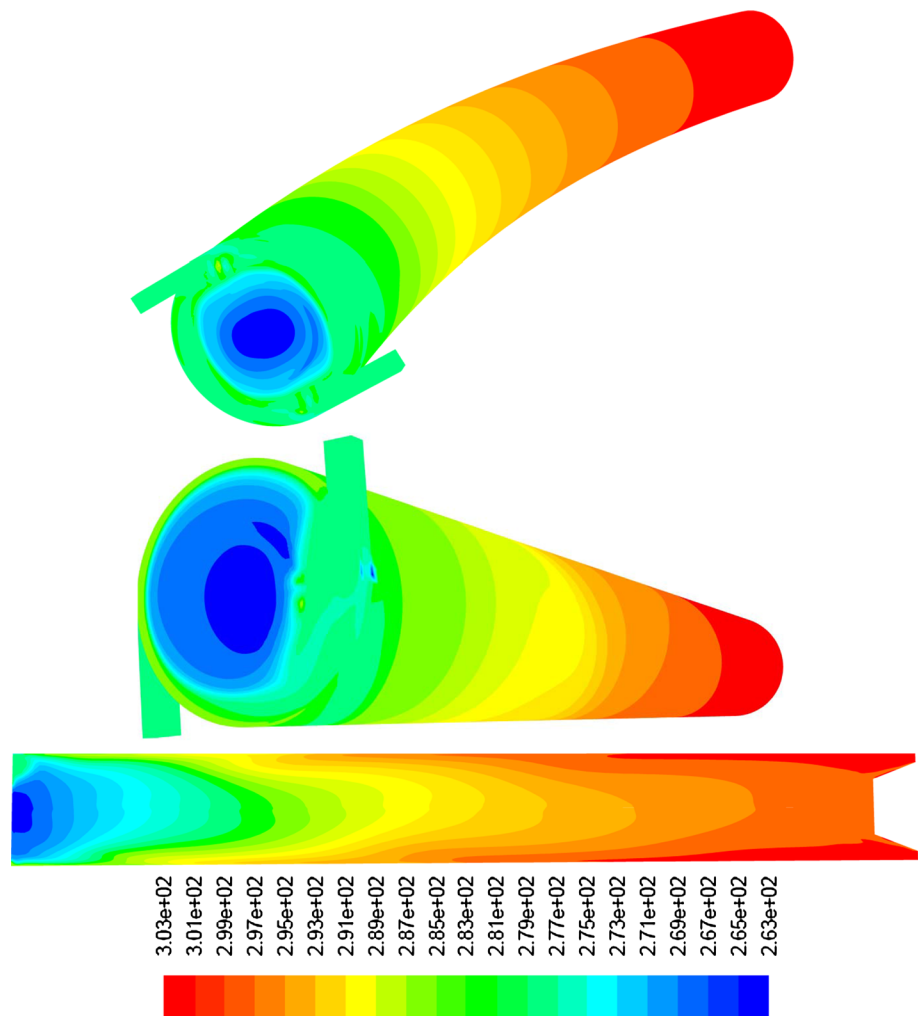
5 Conclusions

The vortex tube efficiency can be improved by utilizing the appropriate bending angle and the experimental tests show that we have an optimum model between $\theta = 0°$ and $\theta = 20°$. Preliminary tests (before the optimization) indicate that the bending angle should be small and not more than 10 under our experimental tests so there is an optimal bending angle of maintube to achieve the highest possible refrigeration performance. The preliminary experimental results indicate that $\theta = 10°$ yield the highest cold temperature reduction, which exceeds straight one by about 8.71 %. In fact the optimum model before the optimization was $\theta = 10°$. The influence of number of nozzles on the cryogenic efficiency relies on the cold mass fraction. Increasing the number of nozzles leads to a severe sensitivity of ΔTc with the variation of the cold mass fraction and achieves the highest possible cold temperature drop ΔTc at lower cold mass fraction as well. The purpose of this investigation was to introduce a 3D CFD model of a vortex tube system for utilize as a design tool in optimizing vortex tube parameters and geometries. The comparison between the 3D CFD results and the measured data yielded promising results relative to the model's ability to predict the fluid treatment. Deviation of the predicted and measured values for the cold temperature difference is less than or equal to 5.96 % (at cold mass fraction of 0.24). Twenty CFD models have been created between $\theta = 0$ and $\theta = 20$ to optimize the bending angle. Experimental and numerical results show that the best candidate for bending angle is $\theta = 16°$ (after optimization) which creates the cold temperature difference equal to 29.69 K and 29.21 K respectively. This results show that this optimization improves the vortex tube performance around 4 % compared to $\theta = 10°$.

References

1. Ranque GJ (1933) Experiments on expansion in a vortex with simultaneous exhaust of hot air and cold air. Le J. de Physique et le Radium 4:112–114

2. Ranque GJ (1934) Method and apparatus for obtaining from a fluid under pressure two outputs of fluid at different temperatures. US Pat 1(952):281
3. Hilsch R (1947) The use of expansion of gases in a centrifugal field as a cooling process. Rev Sci Instrum 18:108–113
4. Valipour MS, Niazi N (2011) Experimental modeling of a curved Ranque–Hilsch vortex tube refrigerator. Int J Refrig 34:1109–1116
5. Dincer K (2011) Experimental investigation of the effects of threefold type Ranque–Hilsch vortex tube and six cascade type Ranque–Hilsch vortex tube on the performance of counter flow Ranque–Hilsch vortex tubes. Int J Refrig 34(6):1366–1371
6. Xue Y, Arjomandi M, Kelso R (2012) Experimental study of the flow structure in a counter flow Ranque–Hilsch vortex tube. Int J Heat Mass Transf 55(21–22):5853–5860
7. Im SY, Yu SS (2012) Effects of geometric parameters on the separated air flow temperature of a vortex tube for design optimization. Energy 37(1):154–160
8. Mohammadi S, Farhadi F (2013) Experimental analysis of a Ranque–Hilsch vortex tube for optimizing nozzle numbers and diameter. Appl Therm Eng 61(2):500–506
9. Rafiee SE, Rahimi M (2013) Experimental study and three-dimensional (3D) computational fluid dynamics (CFD) analysis on the effect of the convergence ratio, pressure inlet and number of nozzle intake on vortex tube performance-Validation and CFD optimization. Energy. doi:10.1016/j.energy.2013.09.060
10. Saidi MH, Yazdi MRA (1999) Exergy model of a vortex tube system with experimental results. Energy 24:625–632
11. Secchiaroli A, Ricci R, Montelpare S, D'Alessandro V (2009) Numerical simulation of turbulent flow in a Ranque–Hilsch vortex tube. Int J Heat Mass Transf 52:5496–5511
12. Shamsoddini R, Nezhad AH (2010) Numerical analysis of the effects of nozzles number on the flow and power of cooling of a vortex tube. Int J Refrig 33:774–782
13. Pinar AM, Uluer O, Kırmaci V (2009) Optimization of counter flow Ranque–Hilsch vortex tube performance using Taguchi method. Int J Refrig 32:1487–1494
14. Chang K, Li Q, Zhou G, Li Q (2011) Experimental investigation of vortex tube refrigerator with a divergent hot tube. Int J Refrig 34:322–327
15. Stephan K, Lin S, Durst M, Seher F, Huang D (1983) An investigation of energy separation in a vortex tube.Int. J Heat Mass Transf 26(3):341–348
16. Dincer K, Baskaya S, Uysal BZ (2008) Experimental investigation of the effects of length to diameter ratio and nozzle number on the performance of counter flow Ranque–Hilsch vortex tubes. Heat Mass Transf 44:367–373
17. Akhesmeh S, Pourmahmoud N, Sedgi H (2008) Numerical study of the temperature separation in the Ranque–Hilsch vortex tube. Am J Eng Appl Sci 3:181–187
18. Gibson MM, Launder BE (1978) Ground effects on pressure fluctuations in the atmospheric boundary layer. J Fluid Mech 86:491–511
19. Launder BE (1989) Second-moment closure: present… and Future? Int J Heat Fluid Flow 10(4):282–300
20. Launder BE, Reece GJ, Rodi W (1975) Progress in the development of a Reynolds-stress turbulence closure. J Fluid Mech 68(3):537–566
21. Yilmaz M, Kaya M, Karagoz S, Erdogan S (2009) A review on design criteria for vortex tubes. Heat Mass Transf 45:613–632
22. Gutsol AF (1997) The Ranque effect. Phys Uspekhi 40:639–658